PERGAMON

International Journal of Heat and Mass Transfer 45 (2002) 1693–1703

International Journal of HEAT and MASS TRANSFER

www.elsevier.com/locate/ijhmt

Direct numerical simulation of turbulent channel flow under stable density stratification

O. Iida [a,*], N. Kasagi [b], Y. Nagano [a]

[a] Department of Mechanical Engineering, Nagoya Institute of Technology, Gokiso-cho, Showa-ku, Nagoya 466-8555, Japan
[b] Department of Mechanical Engineering, University of Tokyo, Bunkyo-ku, Tokyo 113-8656, Japan

Received 8 November 2000; received in revised form 6 July 2001

Abstract

Direct numerical simulations are performed for a fully developed horizontal turbulent channel flow under stable density stratification. The skin-friction and the Nusselt number agree well with the experimental results. Internal gravity waves (IGW) are found to be built up in the core region, where the turbulent heat flux is suppressed drastically and the steep mean velocity and temperature gradients result. In the central region of the channel, the stable density stratification works as the virtual wall to block turbulent heat transfer. It is also found that the energy of IGW is transferred from the shear-induced turbulence through the pressure diffusion. With an increase in the stratification, the flow on one wall starts to become laminar, although it is still turbulent on the other.

1. Introduction

When a flow is driven in the horizontal direction under a gravitational acceleration, it is called a stratified flow. Not only in many important engineering flows, but also in geophysical flows, turbulent heat transport occurs in the presence of unstable or stable density stratification. When unstable stratification is imposed, turbulence activity is enhanced, while under stable stratification, turbulence is suppressed and the flow finally becomes relaminarized. Under stably stratified fluids, internal gravity waves (IGW) are generated by buoyancy. The low temperature and the high-density fluid lifted upward by turbulence may bounce back due to the buoyancy force, causing an oscillation, i.e., IGW [1]. The generation of the wave-like perturbations is observed in the stably stratified boundary layer [2,3]. It is also found that in the linear gravity waves, phase difference between vertical motions and temperature will be $\pm\pi/2$ in their cospectral [4]. As a result, linear IGW do not transfer heat, although they can transfer momentum through the action of pressure force [1]. The experimental results [5] show that $\rho_{v\theta}$ decreases more rapidly than ρ_{uv} when stable density stratification is enhanced.

In the stably stratified boundary layer, IGW are subjected to strong nonlinear interaction with the turbulence [4]. The effects of stratification on turbulence are often investigated through direct numerical simulation (DNS) [6–8] and experiment [9,10] of homogeneous stably stratified flow. There are few results of DNS of the fully developed wall turbulence under stable density stratification [11].

On the other hand, many experiments and atmospheric observations of stratified wall turbulence have been well summarized by Stull [4] and Turner [12]. They showed that the balance between mechanical generation and turbulence dumping due to buoyancy varies from case to case, creating stable boundary layers that range from well mixed to non-turbulent region. This criterion can be determined by using the gradient Richardson number Ri_g. The oceanic and atmospheric observations show that when Ri_g is smaller than the critical value, which is typically 0.25, strong stable density stratification in a turbulent boundary layer induces a steeper mean velocity gradient and generates intermittent

* Corresponding author. Tel.: +81-52-735-5347; fax: +81-52-735-5347.
E-mail address: iida@heat.mech.nitech.ac.jp (O. Iida).

0017-9310/02/$ - see front matter
PII: S0017-9310(01)00271-X

Nomenclature

C_f	friction coefficient, $2\tau_w/\rho U_b^2$
c_p	specific heat at constant pressure
E_{22}	one-dimensional energy spectrum of $\overline{v^{+2}}$
Gr	Grashof number, $g\beta(T_1 - T_0)(2\delta)^3/\nu^2$
g	gravitational acceleration
Nu, Nu^*	Nusselt number, $2\delta q_w/\lambda T_b$, $2\delta q_w/\lambda\Delta T$
Pr	molecular Prandtl numbers, κ/ν
q_w	total heat flux at the wall, $\lambda(\mathrm{d}T/\mathrm{d}y)_w$
Re_b	bulk mean Reynolds number, $2U_b\delta/\nu$
Re_τ	Reynolds number, $u_\tau\delta/\nu$
Ri_g	gradient Richardson number, $g\beta\frac{\mathrm{d}T}{\mathrm{d}y}\Big/\left(\frac{\mathrm{d}U}{\mathrm{d}y}\right)^2$
Ri_b	bulk Richardson number, Gr/Re_b^2
T	temperature
T_0, T_1	temperatures at bottom and top walls
T_b	bulk mean temperature, $(\int_{-\delta}^{0} U(T - T_0)\mathrm{d}y + \int_0^{\delta} U(T_1 - T)\mathrm{d}y)/(2\delta U_b)$
U	mean velocity in x-direction
U_b	bulk mean velocity, $\int_{-\delta}^{\delta} U\mathrm{d}y/2\delta$
u, v, w	fluctuating velocity components in x-, y- and z-directions
u_τ	friction velocity, $\sqrt{\tau_w/\rho}$
p	pressure fluctuation
x, y, z	streamwise, wall-normal and spanwise directions
β	volumetric expansion coefficient
ΔT	temperature difference, $T_1 - T_0$
δ	channel half width
Θ	mean temperature difference, $\overline{T} - T_0$
θ	fluctuating temperature, $T - \overline{T}$
θ_τ	friction temperature, $\left(\frac{\mathrm{d}\Theta}{\mathrm{d}y}\right)_w \nu\Big/ u_\tau Pr$
ν	kinematic viscosity
κ	thermal diffusivity
κ_1	wave number in the streamwise direction
ρ	density
ρ_{uv}	cross correlation between u and v
$\rho_{v\theta}$	cross correlation between θ and v
τ_w	wall shear stress
$(\,)_0$	value at $Gr = 0$ and $Pr = 0.71$
$(\,)_w$	value at the wall
$(\,)^+$	non-dimensionalized by wall variables u_τ, θ_τ and ν
$\overline{(\,)}$	ensemble average

turbulent flow regime due to Kelvin–Helmholz instability [1,12]. In the experiment of the homogeneous shear flow, the critical Ri_g is also found to be 0.25 [9]. On the other hand, in the regime of a large Richardson number, turbulence is significantly suppressed and IGW are the dominant flow structure. As a result, there is a significant interaction between the region of turbulence and IGW in a turbulent boundary layer; it is no longer homogeneous in the vertical direction. Previous studies on turbulent heat and momentum transfer indicate that a pressure-correlation term in the budget of turbulent kinetic energy not only acts to redistribute turbulent kinetic energy, but also drains it out of the turbulent boundary layer through IGW [4]. However, static pressure fluctuations are too difficult to measure both in the atmosphere and the laboratory. Thus, accurate numerical simulations are required to investigate the interaction between turbulence and IGW.

For $Ri_g > 0.25$, turbulence does not exist throughout the entire flow region and a part of the flow field could be relaminarized. Reverse transition from turbulent to laminar flow has been studied by many investigators, since it has a very complex and important nature to many flows [13]. These studies give a fundamental insight how to control turbulence and reduce the drag.

In this study, a series of DNS is carried out for a turbulent channel flow under stable density stratification. Our major objective is to investigate the fundamental effects of stable density stratification on wall shear turbulence. In particular, the interaction between turbulence and IGW, and the relaminarization under strong density stratification are studied in detail. Although almost all experiments and atmospheric observations are on the boundary layer turbulence at the higher Reynolds number, the experiment of Fukui et al. [14] was performed in the turbulent channel flow at relatively low Reynolds number. Our DNS data are in good agreement with Fukui et al. [14] and the homogeneous shear flow [5,6], indicating the validity of our results. Our result showed that IGW are generated and the turbulent heat flux is markedly attenuated in the central region of a channel when Ri_g exceeds 0.25, whereas, in the near-wall region, turbulence still remains the dominant flow structure. Under the strong density stratification, the large-scale turbulence is attenuated over the entire channel. As a result, the flow on one side of the channel becomes relaminarized. The similar relaminarization is observed in DNS of the minimal flow unit [15], where the computational regions are narrowed and the large-scale turbulence is filtered out.

2. Computational conditions of DNS

We study a turbulent flow between two parallel horizontal walls, where the streamwise, wall-normal and

Table 1
Flow conditions for coarse-grid calculations

Case	NC	SC1	SC2	SC3	SC4	SC5
Gr	0	1.3×10^6	4.4×10^6	7.2×10^6	1.0×10^7	2.0×10^7
Re_b	4349	4548	4866	5114	5383	6060
Ri_b	0	0.063	0.18	0.28	0.35	0.54
Re_τ				150		
Pr				0.71		

spanwise directions are denoted x, y, and z, respectively. The flow is driven by a constant mean pressure gradient in the x-direction. Both flow and thermal fields are assumed fully developed, so that periodic boundary conditions are imposed in the x- and z-directions. The no-slip boundary condition is assumed at the two walls, which are kept at different, but uniform temperatures. As a result, there is a constant temperature difference ΔT $(= T_1 - T_0)$ between the top (T_0) and bottom walls (T_1), where $(T_1 - T_0)$ is positive. The gravitational acceleration g in the y-direction causes a stable buoyancy effect.

The governing equations are the standard set of hydrodynamic equations with the assumption of the constant physical properties and the Boussinesq approximation. The Reynolds number, Re_τ, which is based on the friction velocity, u_τ, and channel half width, δ, and the Prandtl number, Pr, are $Re_\tau = 150$ and $Pr = 0.71$, respectively. The resultant bulk Reynolds number, Re_b, is 4560 in the case without buoyancy, which agree well with other DNS results of the same flow geometry [16,17]. In this numerical simulation, the Grashof number, Gr, is increased gradually from 0 to 2×10^7.

Referring to Kim et al. [18], a fourth-order partial differential equation for the velocity v, a second-order partial differential equation for the wall-normal component of vorticity, and the continuity equation are solved to determine the instantaneous flow field. A spectral method is used to obtain the solutions with Fourier series in the x- and z-directions and a Chebyshev polynomial expansion in the y-direction [18]. The energy equation is numerically solved by the similar method used in the equation for the wall-normal component of vorticity [16].

Almost all calculations are carried out with $64 \times 49 \times 64$ (x-, y- and z-directions) grid. In order to assess the numerical accuracy, 128×128 Fourier modes and Chebyshev polynomials up to the 97th order in the wave-number space are used for typical cases of $Gr = 0$, 4.4×10^6 and 1.0×10^7. In all cases, the spanwise period of the computational box is $2\pi\delta$, while the streamwise period is $5\pi\delta$. The results of coarse-grid calculations are qualitatively in reasonable agreement with those of fine-grid ones as is discussed later in both the skin-friction coefficient and the Nusselt number (see Section 3.1). The alternate approaches using the energy spectrum and the mean velocity profile are investigated to show the validity of the coarse-grid calculation by Pan and Banerjee [19] and Iida and Kasagi [20], respectively. Flow conditions of the coarse- and fine-grid DNS are shown in Tables 1 and 2, respectively. The turbulence statistics are calculated as spatio-temporal means after the temporal variation in the mean velocity and temperature profiles have become negligibly small and the flow fields are considered fully developed. In all coarse-grid DNS, the averaging timespan used in obtaining statistics is $1{,}200\, v/u_\tau^2$, except for the case of $Gr = 2.0 \times 10^7$, where averaging is made only over the horizontal domain at some specific time. On the other hand, in the fine-grid DNS, statistics are averaged over a period of $120\, v/u_\tau^2$.

Table 2
Flow conditions for fine-grid calculations

Case	N	S2	S4
Gr	0	4.4×10^6	1.0×10^7
Re_b	4560	5100	5760
Ri_b	0	0.168	0.302
Re_τ		150	
Pr		0.71	

3. Results and discussion

3.1. Effects of stable stratification on turbulent heat and momentum transfer

At first, we discuss the validity of present numerical simulations by comparing our data with the experimental results. Figs. 1 and 2 show the friction coefficient

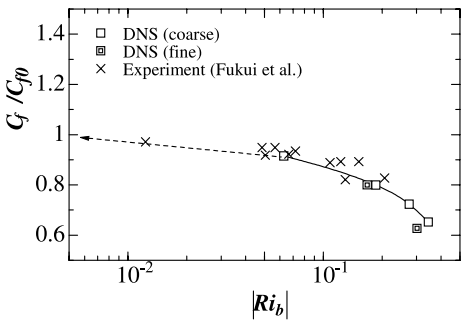

Fig. 1. Distribution of the normalized skin-friction coefficients versus the bulk Richardson number.

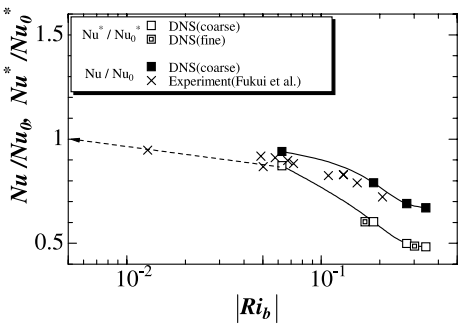

Fig. 2. Distribution of the normalized Nusselt numbers versus the bulk Richardson number.

and the Nusselt number, which are normalized by those of standard channel flow without buoyancy, against the bulk Richardson number $|Gr/Re_b^2|$, respectively. In Fig. 2, two kinds of the Nusselt numbers are plotted. The first one, Nu^*, represents the heat transfer coefficient based on the temperature difference between the two walls, while the other, Nu, is based on the bulk mean temperature as defined in the nomenclatures.

The results of fine-grid DNS agree well with those of coarse-grid in Figs. 1 and 2, indicating the usefulness of the coarse-grid results in exploring a global nature of the flow under study with less computational load. The present results are also in good agreement with the experimental results of Fukui et al. [14]. In the stably stratified channel, both C_f and Nu decrease markedly with the increase in Ri_b. When $Ri_b > 0.54$ ($Gr = 2 \times 10^7$), the flow becomes almost relaminarized. It is also noted that the present DNS and the experimental results [14] have agreed well.

The suppression of heat and momentum transfer due to stable density stratification also contributes to decrease in the correlation coefficients between the wall-normal velocity v and the fluctuations of $-\theta$ and $-u$. Figs. 3(a) and (b) show their correlation coefficients against Ri_g. They are again compared with the experimental results [5] and DNS data [6], both of which are for stably stratified homogeneous shear flows of $Pr = 0.71$. Both correlations decrease strongly with increasing stability, indicating the attenuation of both turbulent heat and momentum transport with increasing stability. Although the experimental ρ_{uv} of Webster [5] show scatter, they also show a reduced degree of correlation with increase of Ri_g. Our data of $\rho_{v\theta}$ are in good agreement with the results of Gerz et al. [6] and Webster [5] in the region of $Ri_g = 0.1$ to 0.25. In the DNS data of smaller Richardson numbers, which correspond to the region near the wall, the viscous effects for low-Reynolds-number flows are significant. This causes scatter in the present data at small Richardson numbers.

Logarithmic plots of mean velocity and temperature distributions are shown in Figs. 4 and 5, respectively. The averaged statistics are symmetric on both walls. In the stably stratified channel, the mean velocity increases in the region $y^+ > 10$. Interestingly, as the thickness of the linear sublayer is increased, the logarithmic region disappears. The disappearance of a logarithmic region is also observed in the DNS of a rotating pipe [21], suggesting an analogy between the effects of rotation and stratification [22]. It is also noted in Fig. 5 that the effects of stratification on the mean temperature distributions are similar to those observed in the mean velocity profiles. The change in the mean temperature profiles is significant in the central region of the channel, because Ri_g is the largest value there.

Figs. 6(a) and (b) show the distributions of the Reynolds shear stress and the turbulent heat flux. When Ri_b increases, $-\overline{v^+\theta^+}$ decreases markedly in the central region of the channel, this is in agreement with the laminar-like steep mean temperature gradient there as shown in Fig. 5. However, the counter-gradient heat flux is not observed when the turbulent heat flux is averaged over the entire x–z plane. On the other hand, the Reynolds shear stress decreases slightly over the entire channel, except very near the wall.

Figs. 7(a) and (b) compare the iso-surfaces of the non-dimensional temperature $(T - T_0)/\Delta T = 0.5$ under neutral and stable density stratification, respectively. A significant difference is observed between these cases. In the case without buoyancy, the temperature iso-surface

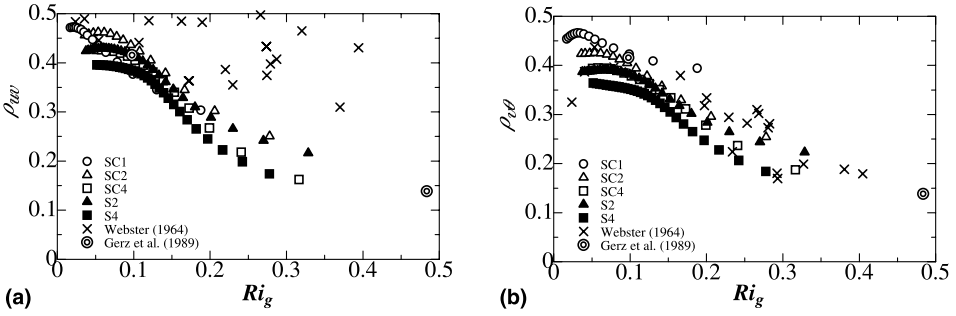

Fig. 3. Correlation between u and v, and v and θ.

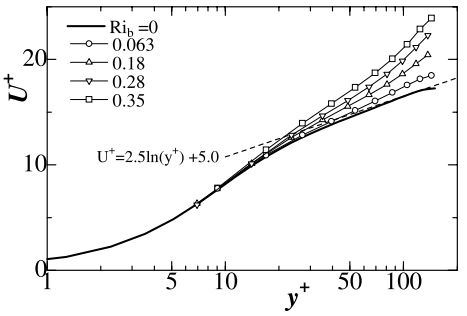

Fig. 4. Logarithmic plot of the mean velocity profile (Case NC, SC1 to SC5).

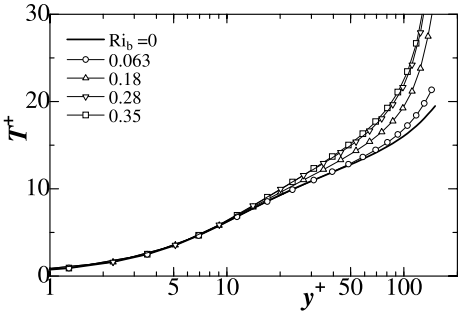

Fig. 5. Logarithmic plot of the mean temperature profile (Case NC, SC1 to SC5).

is violently torn up, indicating that the temperature is effectively mixed by turbulent motions. On the other hand, under stable stratification, undulations of the iso-surface become smaller, and thermal mixing due to turbulence is significantly less. Decreased thermal mixing is consistent with the marked decrease in $-\overline{v^+\theta^+}$ shown in Fig. 6.

3.2. Effects of stratification on turbulence structures

In the following discussion, the change in the turbulence structure is studied through the observation of the instantaneous flow fields and the turbulence statistics. Figs. 8(a) and (b) show a typical example of the velocity vectors in the x–y and y–z planes at $Ri_b = 0.35$ ($Gr = 1 \times 10^7$). The location of x–y and y–z planes included in Figs. 8(a) and (b) are indicated by the black bars in Fig. 9. The iso-surfaces of the pressure fluctuations are also shown in Fig. 8. In Fig. 8(a), a wave-like motion associated with the pressure fluctuation is clearly observed in the central region of the channel. It is noted that a vertically elongated low-pressure region is often generated between the wall and the crest of the wave motions, indicating the close association between them. In this flow, these low pressure regions correspond to the streamwise vortices as shown in the turbulent channel flow without buoyancy [23]. The streamwise vortices reach down near to the wall and are associated with the wave crests as shown in Fig. 8(b). We can also find that these low pressure regions are elongated in the horizontal direction from both Figs. 8(b) and 9.

The distributions of rms velocity fluctuations are shown in Figs. 10(a) and (b). First, we will discuss the case of $0 \leqslant Ri_b \leqslant 0.35$ (see Fig. 10(a)). In the near-wall region $y^+ < 40$, none of the velocity fluctuations are significantly changed, so typical near-wall turbulence is maintained at this Richardson number. In the region $y^+ > 40$, a decrease in v^+_{rms} is observed, while u^+_{rms} increases. This is because the production of u^+_{rms} is enhanced due to the increase in the mean velocity gradient, although $-\overline{u^+v^+}$ decreases. In the central region of the channel, w^+_{rms} decreases markedly. In contrast v^+_{rms} takes a local maximum which is not observed in the neutral flow. That is associated with IGW as discussed later.

As seen from Fig. 10(c), when the bulk Richardson number further increases to 0.54 ($Gr = 2 \times 10^7$), a stable state occurs in which the turbulent flow exists only on one wall ($0 < y^+ < 150$), although on the other wall ($150 < y^+ < 300$) the flow becomes almost relaminarized. These results are similar to those seen in a minimal flow unit [15], where the logarithmic region of the mean velocity profile disappears when the flow became a asymmetric turbulent flow. The disappearance of the logarithmic region is also observed in the present result (see Fig. 4).

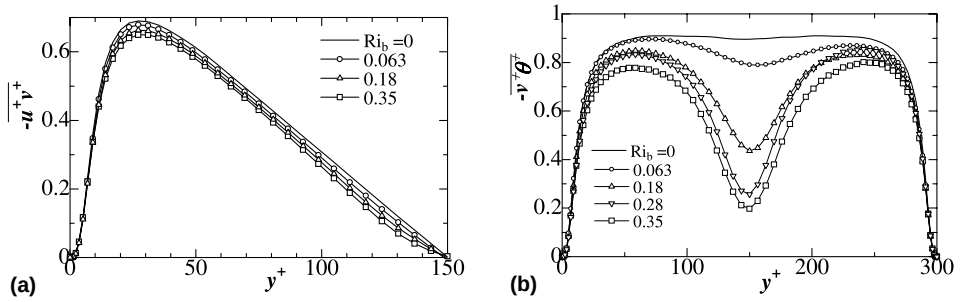

Fig. 6. (a) Distribution of the Reynolds shear stress (Case NC, SC1 to SC5). (b) Distribution of the turbulent heat flux (Case NC, SC1 to SC5).

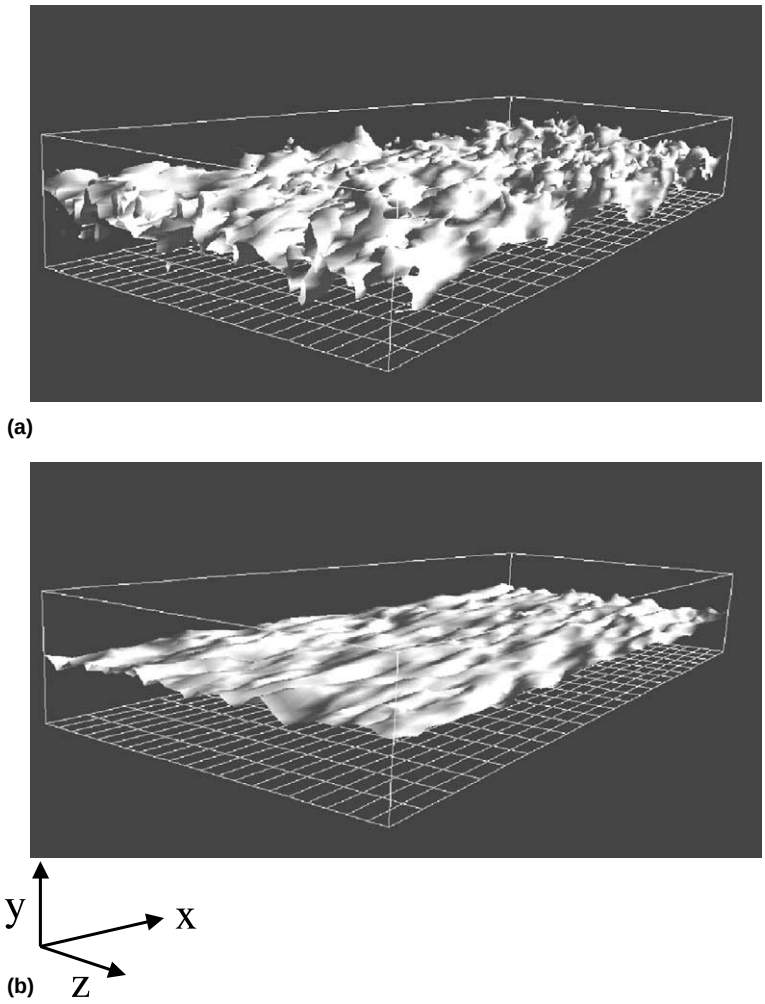

Fig. 7. Iso-surfaces of non-dimensional temperature $(T - T_0)/\Delta T = 0.5$: (a) Case NC, (b) Case SC4.

The distribution of rms temperature fluctuation is shown in Fig. 10(d). In all cases, the peak value exists at the center of the channel, and the increase in θ^+_{rms} with Ri_{b} is largest there. Thus, the effect of buoyancy is strongest in the central region of the channel, and this causes significant decrease in the turbulent heat flux. As discussed later, the budget of the turbulent heat flux also shows the important contribution of the buoyancy dissipation term, i.e., $Gr^+\overline{v^+\theta^+}$. On the other hand, the buoyancy effects are not clearly observed in the rms velocity fluctuations in the channel center in comparison to the temperature fluctuation.

The streamwise energy spectra of wall-normal velocity fluctuations at three typical locations are shown in Fig. 11. Except for the central region of the channel, the energy spectra at low wave numbers decrease with the large-scale turbulent structure being attenuated under stable stratification. This is also the case in the energy spectra of $\overline{u^{+2}}$ and $\overline{w^{+2}}$ (not shown here), although the attenuation of the $\overline{v^{+2}}$ energy spectrum is more significant. Because the buoyancy dissipation in $\overline{v^{+2}}$ is associated with $\overline{v^+\theta^+}$ having its energy at low wave numbers, buoyancy affects the large-scale turbulent structure most seriously.

Another interesting result is that in the central region of the channel, the energy spectrum of $\overline{v^{+2}}$ increases at wave numbers from $k_1 = 1$ to 4. The increase in $\overline{v^{+2}}$ is associated with the generation of IGW as shown in Fig. 12. Fig. 12 shows that the increase in $\overline{v^{+2}}$ occurs at the wave numbers where the phase angle between the wall-normal velocity and the temperature fluctuation is almost $\pi/2$. It is also noted that in the other region of the channel ($y^+ = 10$, 100), their phase angle becomes almost zero, and hence turbulence still remains dominant flow structure rather than IGW.

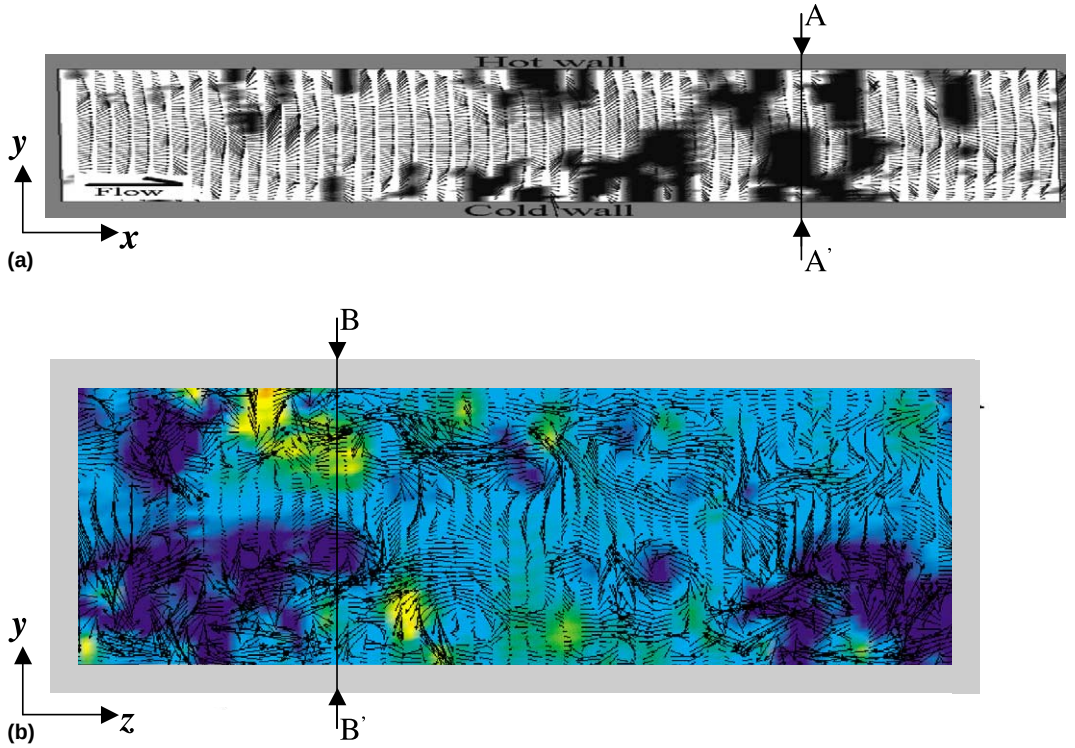

Fig. 8. Instantaneous velocity vectors in the vertical x–y and y–z planes in the stably stratified channel (Case SC4): (a) black to white, $p^+ = -4$ to 0, $\Delta x^+ \times \Delta y^+ = 2356 \times 300$, (b) blue to red, $p^+ = -4$ to 4, $\Delta z^+ \times \Delta y^+ = 942 \times 300$.

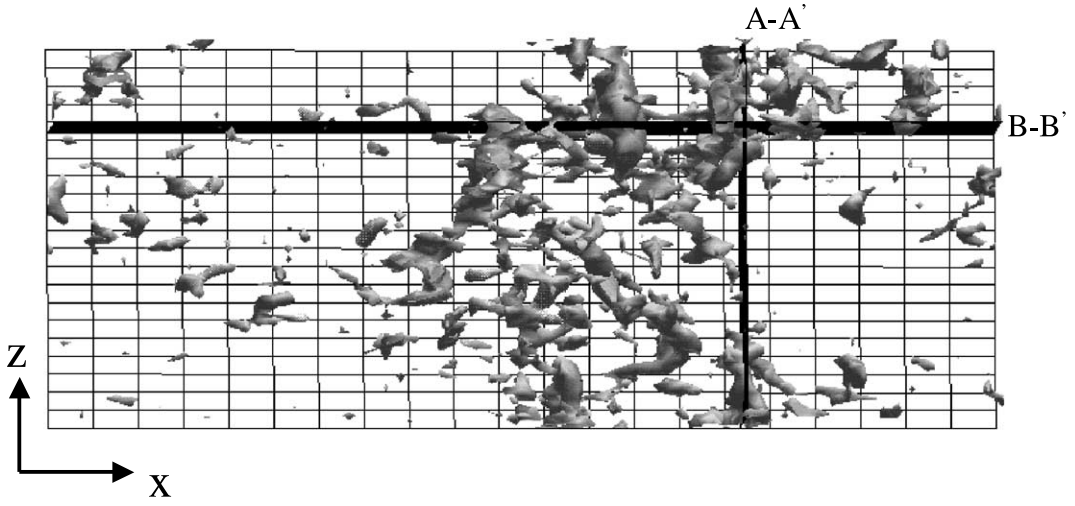

Fig. 9. Instantaneous iso-surfaces of low pressure regions over all the computational region (Case SC4): $p^+ = -4$.

The partition between turbulent and non-turbulent states can be determined by Ri_g. As discussed in the introduction, when Ri_g surpasses the critical value of 0.25, the turbulence is significantly attenuated and IGW become the dominant flow structure [4]. Fig. 13 shows that in the region beyond $y^+ \sim 130$, $Ri_g > 0.25$ in all cases of the stably stratified channel flow studied. This indicates that IGW are the dominant flow structure. In the region of $y^+ < 100$, Ri_g is smaller than 0.25 and shear turbulence is dominant. These results are in accordance with

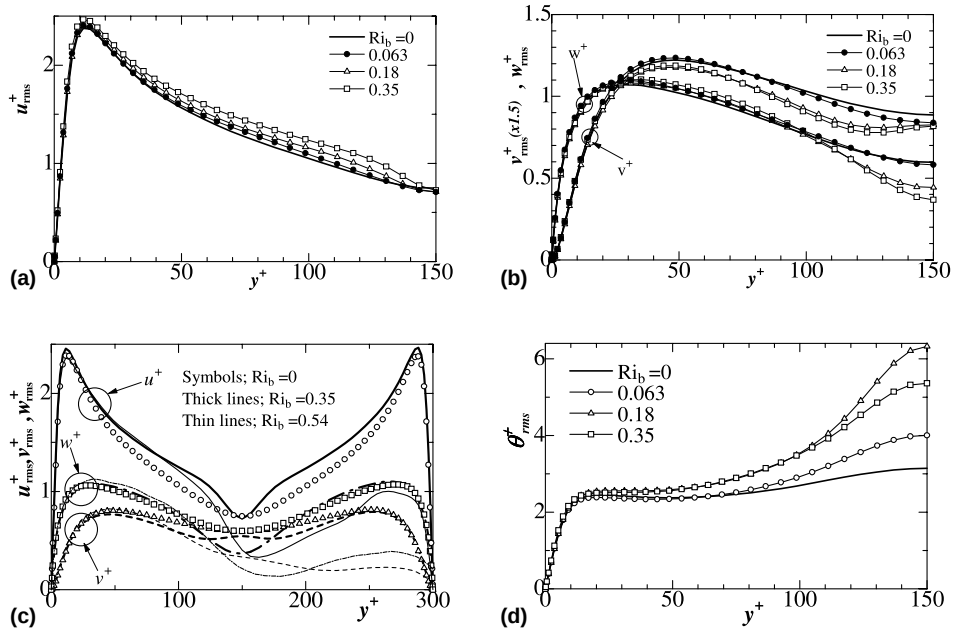

Fig. 10. Distribution of the rms velocity and temperature fluctuations: (a) u^+_{rms} (Case NC, SC1, SC2 and SC4), (b) v^+_{rms}, w^+_{rms} (Case NC, SC1, SC2 and SC4), (c) u^+_{rms}, v^+_{rms} and w^+_{rms} (Case NC, SC4 and SC5), (d) θ^+_{rms}.

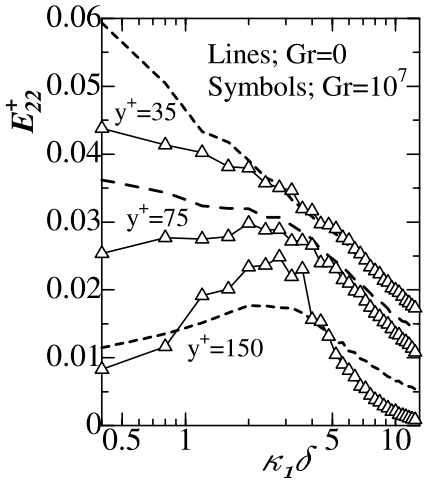

Fig. 11. Streamwise energy spectra of $\overline{v^{+2}}$ (Case SC4).

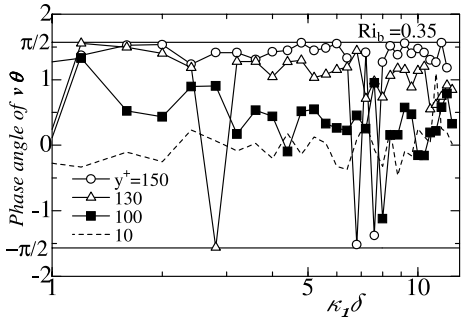

Fig. 12. The phase angle between the wall-normal velocity and temperature fluctuations (Case SC4).

the instantaneous flow structure shown in Figs. 8(a) and (b) and the distribution of the phase angle shown in Fig. 12.

3.3. Effects of stratification on budgets of turbulent kinetic energy and turbulent heat flux

In the following section, we discuss the transport mechanisms of turbulent kinetic energy and turbulent heat flux, which interact each other through the buoyancy dissipation term and the mean temperature gradient. The budget equation of turbulent kinetic energy $\overline{u_i u_i}/2$ is given as

$$0 = \underbrace{-\overline{u^+v^+}\frac{dU}{dy}}_{\text{Production}} \underbrace{+Gr^+\overline{v^+\theta^+}}_{\text{Buoyancy dissipation}} \underbrace{-\overline{\frac{\partial u_j^+}{\partial x_i^+}\frac{\partial u_j^+}{\partial x_i^+}}}_{\text{Dissipation}}$$
$$\underbrace{-\frac{\partial}{\partial y^+}\overline{v^+\frac{u_i^+u_i^+}{2}}}_{\text{Turbulent diffusion}} \underbrace{+\frac{\partial^2}{\partial y^{+2}}\overline{\frac{u_i^+u_i^+}{2}}}_{\text{Viscous diffusion}} \underbrace{-\frac{\partial}{\partial y^+}\overline{p^+v^+}}_{\text{Pressure diffusion}}. \quad (1)$$

Only the buoyancy dissipation term is directly affected by buoyancy. This term is also included in the budget

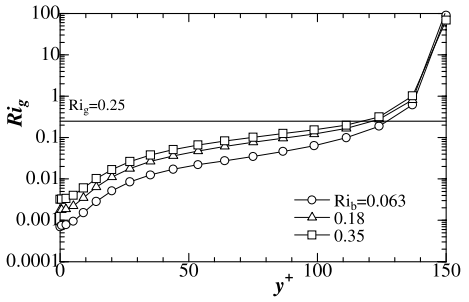

Fig. 13. The distribution of the gradient Richardson numbers (Case SC1, SC2, SC4 and SC5).

equation of the vertical component of the Reynolds normal stresses, but not related to the other components. The budget equation of the Reynolds normal stress $\overline{v^{+2}}$ is given as

$$0 = \underbrace{2Gr^{+}\overline{v^{+}\theta^{+}}}_{\text{Buoyancy dissipation}} \underbrace{+2\overline{p^{+}\left(\frac{\partial u^{+}}{\partial y^{+}}+\frac{\partial v^{+}}{\partial x^{+}}\right)}}_{\text{Pressure–strain correlation}} \underbrace{-2\overline{\frac{\partial v^{+}}{\partial x_i^{+}}\frac{\partial v^{+}}{\partial x_i^{+}}}}_{\text{Dissipation}}$$
$$\underbrace{-\frac{\partial}{\partial y^{+}}\overline{v^{+3}}}_{\text{Turbulent diffusion}} \underbrace{+\frac{\partial^2}{\partial y^{+2}}\overline{v^{+2}}}_{\text{Viscous diffusion}} \underbrace{-2\frac{\partial}{\partial y^{+}}\overline{p^{+}v^{+}}}_{\text{Pressure diffusion}}. \quad (2)$$

Figs. 14 and 15 show the dominant terms of turbulent kinetic energy and $\overline{v^{+2}}$. In Fig. 14, the buoyancy dissipation term is negligibly small in comparison to the production and dissipation terms, both of which decrease in almost all region channel. The enhanced mean velocity gradient increases the production term in the near-wall region, $y^{+} < 15$, which balances with the increase in the turbulent diffusion. In the region away from the wall, $20 < y^{+}$, the decrease in the production term almost balances with the decrease in the dissipation term. Fig. 15(a) shows that the buoyancy dissipation term almost balances with the increase in the pressure–strain correlation term over the entire channel except near the wall. Thus, the intercomponent energy transfer from the streamwise to the wall-normal velocity fluctuations is enhanced by the suppression of the wall-normal velocity due to buoyancy. In Fig. 15(b), the distributions of the pressure and turbulent diffusion terms change significantly in the central region of the channel. The turbulent diffusion term decreases to nearly zero in the central region of a channel. It can be seen that through the pressure-diffusion term, the turbulent kinetic energy $\overline{v^{+2}}$ is transported from the near-wall region to the channel center where IGW become the dominant flow structure.

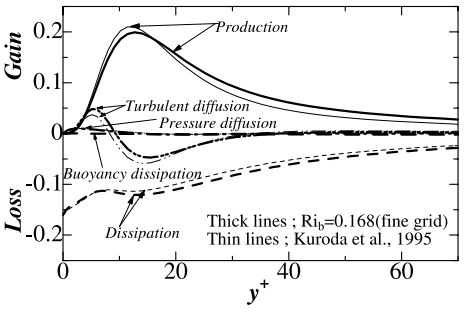

Fig. 14. Budget of turbulent kinetic energy (Case S2).

The individual terms in the budget of $\overline{v^{+}\theta^{+}}$ are written as

$$0 = \underbrace{Gr^{+}\overline{\theta^{+2}}}_{\text{Buoyancy dissipation}} \underbrace{-\overline{v^{+2}}\frac{\mathrm{d}\Theta^{+}}{\mathrm{d}y^{+}}}_{\text{Production}} \underbrace{+\overline{p^{+}\frac{\partial\theta^{+}}{\partial y^{+}}}}_{\text{Pressure scrambling}}$$
$$\underbrace{-\left(1+\frac{1}{Pr}\right)\overline{\frac{\partial v^{+}}{\partial x_i^{+}}\frac{\partial\theta^{+}}{\partial x_i^{+}}}}_{\text{Dissipation}} \underbrace{-\frac{\partial}{\partial y^{+}}\overline{v^{+2}\theta^{+}}}_{\text{Turbulent diffusion}}$$
$$\underbrace{+\frac{\partial}{\partial y^{+}}\left(\overline{\theta^{+}\frac{\partial v^{+}}{\partial y^{+}}}+\frac{1}{Pr}\overline{v^{+}\frac{\partial\theta^{+}}{\partial y^{+}}}\right)}_{\text{Viscous diffusion}} \underbrace{-\frac{\partial}{\partial y^{+}}\overline{p^{+}v^{+}}}_{\text{Pressure diffusion}}, \quad (3)$$

and the dominant terms in Eq. (3) are shown in Fig. 16. The dominant source term of $v^{+}\theta^{+}$ is the production term, $-\overline{v^{+2}}\mathrm{d}\Theta^{+}/\mathrm{d}y^{+}$, while the pressure-scrambling term contributes mainly to the destruction of the turbulent

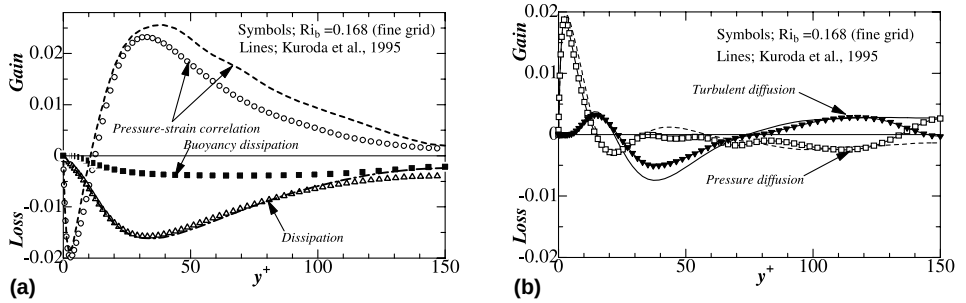

Fig. 15. Budget of $\overline{v^{+2}}$ (Case S2).

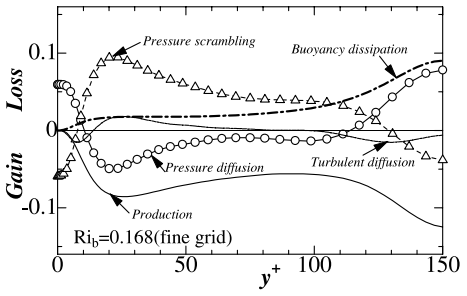

Fig. 16. Budget of $\overline{v^+\theta^+}$ (Case N and S2).

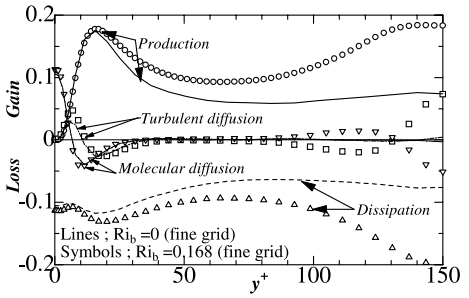

Fig. 17. Budget of $\overline{\theta^{+2}}/2$ (Case N and S2).

heat flux. However, in the near-wall region where the blocking effect suppresses the turbulent heat flux, the pressure-scrambling and pressure-diffusion terms become the dominant source and sink terms, respectively. For stable stratification, the most serious effects appear in the central region of the channel where the buoyancy dissipation term $Gr^+\overline{\theta^{+2}}$ is the largest, and hence the turbulent heat flux is damped. Moreover, in that region, the distributions of the pressure-scrambling, pressure-diffusion and turbulent-diffusion terms become qualitatively similar to those in the near-wall region. This suggests that the blocking effects due to the stable stratification affect the transport of turbulent heat flux. Hence, stable stratification works as the virtual adiabatic wall for the turbulent heat flux. It should also be noted that in the same region, the production of $\overline{v^+\theta^+}$ increases markedly because of the steeper mean temperature gradient there (e.g., Fig. 5). However, the production of $\overline{v^+\theta^+}$ is almost balanced by the buoyancy dissipation term. The residual of $\overline{v^+\theta^+}$ is transported into the near-wall region through the pressure diffusion. This is in contrast to the $\overline{v^{+2}}$ budget, where the pressure diffusion transports the turbulence energy into the central region of the channel.

As discussed in Fig. 8, the streamwise vortices associated with the low pressure are concentrated in both vertically and horizontally elongated regions between IGW and the wall. These vortices must contribute to the pressure-associated interaction between the near-wall region and the channel center.

Finally, the transport mechanism of the variance of the temperature fluctuation $\overline{\theta^{+2}}/2$ is studied. The budget equation of the temperature variance $\overline{\theta^{+2}}/2$ is given as

$$0 = \underbrace{-\overline{v^+\theta^+}\frac{\mathrm{d}\Theta^+}{\mathrm{d}y^+}}_{\text{Production}} \underbrace{-\frac{\partial}{\partial y^+}\overline{v^+\frac{\theta^{+2}}{2}}}_{\text{Turbulent diffusion}} \underbrace{+\frac{1}{Pr}\frac{\partial^2}{\partial y^{+2}}\frac{\overline{\theta^{+2}}}{2}}_{\text{Molecular diffusion}} \underbrace{-\frac{1}{Pr}\overline{\frac{\partial\theta^+}{\partial x_i^+}\frac{\partial\theta^+}{\partial x_i^+}}}_{\text{Dissipation}}. \tag{4}$$

The results are shown in Fig. 17. A significant increase in both production and dissipation is found over the entire region of the channel. The increase in the mean temperature gradient results in the increase in the production, which still balances with the dissipation. It is also found that the turbulent-diffusion term transfers the temperature fluctuation from the central region of the channel, i.e., the peak location of the production of $\overline{\theta^{+2}}/2$, to the logarithmic region. On the other hand, the molecular diffusion is balanced with the turbulent diffusion.

4. Conclusions

A series of DNSs is performed for a fully developed horizontal turbulent channel flow under stable density stratification. By investigating the basic turbulence statistics, their budget and the instantaneous turbulent structure, the following conclusions are obtained.

Both Nusselt number and skin-friction coefficient decrease as stable stratification is imposed, and this result is in good agreement with the experimental results. The correlations between the velocity and temperature fluctuations are also suppressed. Under stable density stratification, the linear sublayer and the buffer region increase and the logarithmic region is less developed. This results in the significant decrease in both the Nusselt number and the skin-friction coefficient.

In the core region of a channel where $Ri_g > 0.25$, turbulence is significantly suppressed and IGW become the dominant flow structures. Thus, the turbulent heat flux decreases markedly resulting in a steep mean temperature gradient. Qualitative similarity is found between the near-wall and channel central regions in the transport mechanism of the turbulent heat flux. Namely, stable stratification works as the virtual adiabatic wall for the turbulent heat flux in the central region of a channel. On the other hand, near the wall where $Ri_g < 0.25$, shear turbulence still dominates. The turbulent kinetic energy is transferred to the channel center through the pressure diffusion, while the turbulent heat flux is transferred from the channel center to the near-wall region due to the pressure diffusion. Instantaneous turbulent structure shows that the streamwise vortices associated with the low pressure are concentrated in both vertically and horizontally elon-

gated regions between the IGW and the wall. These vortices must contribute to the pressure-associated interaction between the near-wall region and the channel center. It is also found that in this low-Reynolds-number flow, the gradient Richardson number and the critical Richardson number are still useful parameters to determine the flow structure under stable density stratification.

In the stably stratified flow, turbulence at low wave numbers is attenuated while it is maintained at high wave numbers. Thus, strong density stratification has the same effects as decreasing the computational region. When stratification becomes stronger, the flow on one wall becomes laminar as in the minimal flow unit, although it remains turbulent on the other wall.

Acknowledgements

This work was supported by the Ministry of Education, Science, Sports and Culture through Grant-in-Aid for Scientific Research (B) (No. 10450085). We also wish to thank the referees for their helpful comments and suggestions. The DNS data in the present study is available from the website at http: /www.thtlab.u-tokyo.ac.jp/.

References

[1] D.J. Tritton, Physical Fluid Dynamics, Oxford University Press, London, 1988 (Chapters 15, 21).
[2] E.E. Gossard, W.H. Hooke, Waves in the Atmosphere, Atmospheric Infrasound and Gravity Waves – their Generation and Propagation, Elsevier, Amsterdam, 1975 (Chapter 10).
[3] W.H. Hooke, R.M. Jones, Dissipative waves excited by gravity wave encounters with the stably stratified planetary boundary layer, J. Atmos. Sci. 43 (1986) 2048–2060.
[4] R.B. Stull, An Introduction to Boundary Layer Meteorology, Kluwer Academic Publishers, Dordrecht, 1988 (Chapters 5, 12).
[5] C.A.G. Webster, An experimental study of turbulence in a density stratified shear flow, J. Fluid Mech. 19 (1964) 221–245.
[6] T. Gerz, U. Schumann, S.E. Elghobashi, Direct numerical simulation of stratified homogeneous turbulent shear flows, J. Fluid Mech. 200 (1989) 563–594.
[7] S.E. Holt, J.R. Koseff, J.H. Ferziger, A numerical study of the evolution and structure of homogeneous stably stratified turbulence, J. Fluid Mech. 237 (1992) 499–539.
[8] F.G. Jacobitz, S. Sarkar, C.W. Van Atta, Direct numerical simulations of the turbulence evolution in a uniformly sheared and stably stratified flow, J. Fluid Mech. 342 (1997) 231–261.
[9] J.I. Rohr, E.C. Itsweire, K.N. Helland, C.W. Van Atta, Growth and decay of turbulence in a stably stratified shear flow, J. Fluid Mech. 195 (1988) 77–111.
[10] S.P.S. Piccirillo, C.W. Van Atta, The evolution of a uniformly sheared thermally stratified turbulent flow, J. Fluid Mech. 195 (1997) 61–86.
[11] G.N. Coleman, J.H. Ferziger, P.R. Spalart, Direct simulation of the stably stratified turbulent Ekman layer, J. Fluid Mech. 244 (1992) 677–712.
[12] J.S. Turner, Buoyancy Effects in Fluids, Cambridge University Press, Cambridge, 1973.
[13] R. Narashimha, K.R. Sreenivasan, Relaminarization of fluid flows, Adv. Appl. Mech. 19 (1979) 221–309.
[14] K. Fukui, M. Nakajima, H. Ueda, A laboratory experiment on momentum and heat transfer in the stratified surface layer, Quart. J. R. Met. Soc. 109 (1983) 661–676.
[15] J. Jimenez, P. Moin, The minimal flow unit in near-wall turbulence, J. Fluid Mech. 225 (1991) 213–241.
[16] N. Kasagi, Y. Tomita, A. Kuroda, Direct numerical simulation of passive scalar field in a turbulent channel flow, ASME J. Heat Trans. 114 (1992) 598–606.
[17] A. Kuroda, N. Kasagi, M. Hirata, Direct numerical simulation of turbulent plane Couette–Poiseuille flow: effects of mean shear rate on the near-wall turbulence structures, in: F. Durst, N. Kasagi, B.E. Launder, F.W. Schmit, K. Suzuki, J.H. Whitelaw (Eds.), Turbulent Shear Flows, vol. 9, Springer, Berlin, 1995, pp. 241–257.
[18] J. Kim, P. Moin, R. Moser, Turbulence statistics in fully developed channel flow at low Reynolds number, J. Fluid Mech. 177 (1987) 133–166.
[19] Y. Pan, S. Banerjee, A numerical study of free-slip turbulence in channel flow, Phys. Fluids 7 (1995) 1649–1664.
[20] O. Iida, N. Kasagi, Direct numerical simulation of unstably stratified turbulent channel flow, ASME J. Heat Trans. 119 (1997) 53–61.
[21] P. Orlandi, M. Fatica, Direct simulations of turbulent flow in a pipe rotating about its axis, J. Fluid Mech. 343 (1997) 43–72.
[22] P. Bradshaw, The analogy between streamline curvature and buoyancy in turbulent shear flow, J. Fluid Mech. 36 (1969) 177–191.
[23] N. Kasagi, Y. Sumitani, Y. Suzuki, O. Iida, Kinematics of the quasi-coherent vortical structure in near-wall turbulence, Int. J. Heat Fluid Flow 16 (1995) 2–10.